Adaptive Trim and Trajectory Following for a Tilt-Rotor Tricopter

Ahmad Ansari, Anna Prach, and Dennis S. Bernstein

Abstract— We apply adaptive control to an unconventional aircraft, namely, a three-rotor flight vehicle, one of whose rotors can tilt about the longitudinal axis of the fuselage. This combination of actuators has aerodynamic advantages but also poses challenges in terms of trimming the aircraft in order to balance the torque about the roll, pitch, and yaw axes. The paper uses retrospective cost adaptive control (RCAC) to trim the aircraft in hover as well as to follow straight-line and circular flight trajectories.

I. Introduction

Aircraft flight control is undoubtedly one of the most successful areas of application of feedback control techniques. In particular, adaptive control has a long history of application to aircraft flight control [1], and recent developments show promise for future applications [2]. The underlying motivation for adaptive control is the need for flight safety under off-nominal conditions. Although flight control laws intended for normal operation are thoroughly tested before certification, adaptive control can potentially enhance safety in the presence of faulty sensors and actuators, as well as aerodynamic uncertainty due to off-nominal flight conditions.

An alternative motivation for adaptive flight control is the need to control unconventional aircraft. An unconventional aircraft configuration, in terms of aerodynamics or sensor/actuator configuration, requires detailed modeling followed by trim analysis and finally autopilot design. In this direction, adaptive control can facilitate the analysis of new aircraft configurations by "flying" the aircraft in simulation and allowing the adaptive control law to adjust itself to the dynamics of the vehicle. The resulting performance can suggest limitations of the design as well as the feasibility of adaptive control on the real vehicle.

This paper considers a tilt-rotor tricopter (TRT) aircraft [3]. Unlike a conventional quadrotor, with four propellers, the TRT has three rotors, one of which has the ability to rotate about the longitudinal axis of the aircraft. This configuration saves weight and energy, but poses new control challenges. To address these challenges, we apply retrospective cost adaptive control (RCAC) by "flying" the aircraft in simulation to determine the essential modeling information as well as the resulting performance. RCAC is developed in [4], [5], an overview is given in [6], and application to the NASA GTM model is considered in [7]–[9].

II. Equations of Motion and Trim Analysis

In the tilt-rotor tricopter (TRT), shown in Fig. 1, two propellers rotate in opposite directions compensating the torque, and the third propeller is tilted by a servo motor in order to compensate for the adverse yaw.

A. Ansari and D. S. Bernstein are with the Aerospace Eng. Dept., Univ. Michigan, Ann Arbor, MI. ansahmad@umich.edu. A. Prach is with the National University of Singapore. annaprach@me.com
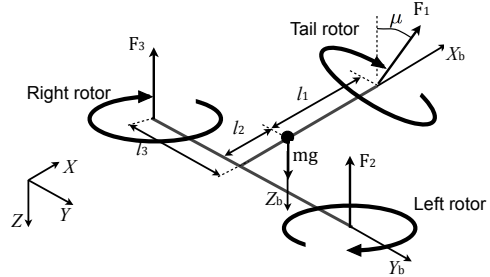
Fig. 1: Tilt-rotor tricopter configuration

A. Nonlinear Equations of Motion

The translational and rotational equations of motion of the TRT, derived in the body frame under a rigid body assumption, neglecting the gyroscopic moments due to the rotors' inertia, drag forces, and moments, and induced pitching moment by the tilted rotor, are given by [10]

$$\dot{u} = rv - qw - g\sin\theta + \frac{F_x}{m}, \tag{1}$$

$$\dot{v} = -ru + pw + g\cos\theta\sin\phi + \frac{F_y}{m}, \tag{2}$$

$$\dot{w} = qu - pv + g\cos\theta\cos\phi + \frac{F_z}{m}, \tag{3}$$

$$\dot{p} = \frac{I_{yy} - I_{zz}}{I_{xx}}qr + \frac{M_x}{I_{xx}}, \tag{4}$$

$$\dot{q} = \frac{I_{zz} - I_{xx}}{I_{yy}}pr + \frac{M_y}{I_{yy}}, \tag{5}$$

$$\dot{r} = \frac{I_{yy} - I_{xx}}{I_{zz}}pq + \frac{M_z}{I_{zz}}, \tag{6}$$

where the 3-2-1 Euler angles ϕ, θ, ψ define the roll, pitch, and yaw, and F_x, F_y, F_z and M_x, M_y, M_z are the components of the aerodynamic force and moment generated by the rotors in the x, y, and z-body directions. The relation between the Euler rates $\dot{\phi}, \dot{\theta}, \dot{\psi}$, and angular body rates p, q, r, which are resolved in the body frame, is given by

$$\begin{bmatrix} \dot{\phi} \\ \dot{\theta} \\ \dot{\psi} \end{bmatrix} = \begin{bmatrix} 1 & \sin\phi\tan\theta & \cos\phi\tan\theta \\ 0 & \cos\phi & -\sin\phi \\ 0 & \frac{\sin\phi}{\cos\theta} & \frac{\cos\phi}{\cos\theta} \end{bmatrix} \begin{bmatrix} p \\ q \\ r \end{bmatrix}. \tag{7}$$

The position of the TRT in the inertial (navigation) frame is defined by the coordinates X, Y, Z.

Assuming constant air density, the aerodynamic force and moment produced by the ith rotor are given by

$$F_i = K_F\Omega_i^2, \quad M_i = K_M\Omega_i^2, \tag{8}$$

where K_F and K_M are the aerodynamic force and moment constants, respectively. The components of the aerodynamic force are given by

$$F_x = 0, \quad F_y = F_1\sin\mu = K_F\Omega_1^2\sin\mu, \tag{9}$$

$$F_z = -(F_1\cos\mu + F_2 + F_3) = -K_F(\Omega_1^2\cos\mu + \Omega_2^2 + \Omega_3^2).$$

Assuming clockwise rotation for the right and tail rotors, and counterclockwise for the left rotor, the aerodynamic moment components are given by [3]

$$M_x = -l_3(F_2 - F_3) = -l_3 K_F(\Omega_2^2 - \Omega_3^2), \qquad (10)$$

$$M_y = -l_2(F_2 + F_3) + l_1 F_1 \cos\mu$$
$$= -l_2 K_F(\Omega_2^2 + \Omega_3^2) + l_1 K_F \Omega_1^2 \cos\mu, \qquad (11)$$

$$M_z = l_1 F_1 \sin\mu - M_1 \cos\mu + M_2 - M_3 \qquad (12)$$
$$= l_1 K_F \Omega_1^2 \sin\mu - K_M \Omega_1^2 \cos\mu + K_M \Omega_2^2 - K_M \Omega_3^2,$$

where the distances l_1, l_2, l_3 are shown in Fig. 1. The parameters of the tilt-rotor tricopter considered in this study are given in Table I [3].

TABLE I: Tricopter parameters

Parameter	Value	Unit
m	1.1	kg
I_{xx}	0.0239	kg-m^2
I_{yy}	0.01271	kg-m^2
I_{zz}	0.01273	kg-m^2
l_1	0.2483	m
l_2	0.1241	m
l_3	0.2150	m
K_F	1.970×10^{-6}	N/rpm^2
K_M	2.880×10^{-7}	N-m/rpm^2

B. Trim Analysis

In the trim analysis, we consider the hover condition. By equating the total force and moment to zero, we establish analytical expressions for the corresponding control inputs and states. The total force F_{total} acting on the TRT is

$$F_{\text{total}} = [F_{\text{total}_x} \; F_{\text{total}_y} \; F_{\text{total}_z}]^{\text{T}}, \qquad (13)$$

where

$$F_{\text{total}_x} = -mg\sin\theta, \qquad (14)$$

$$F_{\text{total}_y} = mg\sin\phi\cos\theta + K_F\Omega_1^2\sin\mu, \qquad (15)$$

$$F_{\text{total}_z} = mg\cos\phi\cos\theta - K_F(\Omega_1^2\cos\mu + \Omega_2^2 + \Omega_3^2). \qquad (16)$$

The total moment M_{total} is given by

$$M_{\text{total}} = [M_x \; M_y \; M_z]^{\text{T}}, \qquad (17)$$

where M_x, M_y, M_z are defined by (10), (11), (12).

In hover, the gravitational force is compensated by the vertical component of the combined thrust produced by all three rotors. The reaction torques on the TRT generated by the left and right rotors are equal and opposite, and thus cancel each other. The reaction torque on the TRT produced by the tail rotor is compensated by tilting the tail rotor about the longitudinal axis by the angle μ as shown in Fig. 1. However, the nonzero tilt angle leads to a nonzero side force. The force is compensated by a nonzero roll angle, which, due to the left and right rotors, produces a horizontal force, which, in turn, requires compensation by the tilt rotor.

In hover, the translational and rotational velocities are equal to zero, that is, $[u \; v \; w]^{\text{T}}_{\text{trim}} = 0$ and $[p \; q \; r]^{\text{T}}_{\text{trim}} = 0$. Then, equating the left hand sides of the total force (14)–(16) and total moment equations (10)–(12) to zero, and solving

for the unknown inputs and states, yields the pitch and roll trim angles and trim controls

$$\phi_{\text{trim}} = \tan^{-1}\Big[-\frac{l_2 K_M}{l_1(l_1 + l_2)K_F}\Big], \quad \theta_{\text{trim}} = 0, \quad (18)$$

$$\mu_{\text{trim}} = \tan^{-1}\Big[\frac{K_M}{l_1 K_F}\Big], \qquad (19)$$

$$\Omega_{1,\text{trim}} = \sqrt{\frac{l_2 g m}{(l_1 + l_2)K_F}\frac{\cos\phi_{\text{trim}}}{\cos\mu_{\text{trim}}}}, \qquad (20)$$

$$\Omega_{2,\text{trim}} = \sqrt{\frac{l_1 g m}{2(l_1 + l_2)K_F}\cos\phi_{\text{trim}}}, \quad \Omega_{3,\text{trim}} = \Omega_{2_{\text{trim}}}.$$

For the given TRT configuration, numerical trim values are given in Table II.

TABLE II: Trim values

Parameter	Value	Units
ϕ_{trim}	-11.10	deg
θ_{trim}	0	deg
μ_{trim}	30.49	deg
$\Omega_{1,\text{trim}}$	1441	rpm
$\Omega_{2,\text{trim}}$	1338	rpm
$\Omega_{3,\text{trim}}$	1338	rpm

C. Actuator Constraints

The actuator constraints are defined by physical limitations such as the min/max rotor speed and the min/max tilt angle. The assumed constraints on the rotors' rpm and tilt angle are

$$0 < \Omega_i < 2\Omega_{i_{\text{trim}}}, \quad -\pi/2 < \mu < \pi/2. \qquad (21)$$

III. CONTROL SYSTEM ARCHITECTURE

We consider an inner-outer-loop control scheme for trajectory following of the TRT as shown in Fig. 2. The outer-loop consists of three PID controllers for following $[X \; Y \; Z]^{\text{T}}$ reference commands. The PID controllers generate references θ_{ref} for the pitch angle, ϕ_{ref} for the roll angle, and w_{ref} for the z-body velocity, which are then fed into the inner-loop retrospective cost adaptive controller (RCAC) as reference commands. In the inner loop, RCAC generates the conventional input Δu_δ by minimizing the inner-loop command-following errors. The control allocation algorithm maps the conventional input Δu_δ to the manipulated input u_{m}, where the manipulated inputs to the TRT are the RPM's $\Omega_1, \Omega_2, \Omega_3$ of the rotors and the tilt angle μ. The conventional and manipulated control inputs are discussed below.

A. Control Allocation

The control allocation algorithm relates control inputs that are similar to conventional helicopter controls, that is, collective δ_{col}, longitudinal δ_{lon}, lateral δ_{lat}, and pedal δ_{ped}, to the manipulated (direct) inputs. The collective input δ_{col} is related to the altitude control; the longitudinal and lateral inputs δ_{lon} and δ_{lat} are related to the pitch and roll control; and the pedal input δ_{ped} is used to control the yaw rate.

Let $u_{\text{m}} \triangleq [\Omega_1^2 \; \Omega_2^2 \; \Omega_3^2 \; \mu]^{\text{T}}$ denote the vector of manipulated inputs, and define the conventional control vector

$$u_\delta \triangleq [\delta_{\text{col}} \; \delta_{\text{lon}} \; \delta_{\text{lat}} \; \delta_{\text{ped}}]^{\text{T}}, \qquad (22)$$
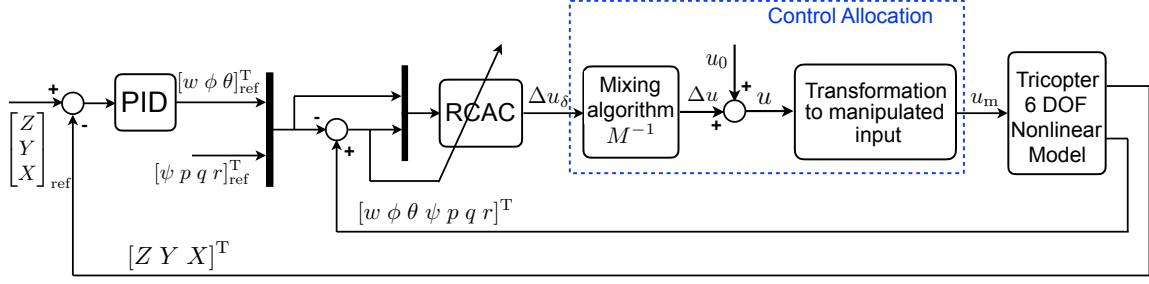
Fig. 2: Controller System Architecture

where

$$\delta_{\mathrm{col}} \triangleq -K_{\mathrm{F}}\Omega_2^2 - K_{\mathrm{F}}\Omega_3^2 - K_{\mathrm{F}}\Omega_1^2\cos\mu, \tag{23}$$

$$\delta_{\mathrm{lon}} \triangleq -l_2 K_{\mathrm{F}}(\Omega_2^2 + \Omega_3^2) + l_1 K_{\mathrm{F}}\Omega_1^2\cos\mu, \tag{24}$$

$$\delta_{\mathrm{lat}} \triangleq -l_3 K_{\mathrm{F}}(\Omega_2^2 - \Omega_3^2), \tag{25}$$

$$\delta_{\mathrm{ped}} \triangleq l_1 K_{\mathrm{F}}\Omega_1^2\sin\mu - K_{\mathrm{M}}\Omega_1^2\cos\mu + K_{\mathrm{M}}\Omega_2^2 - K_{\mathrm{M}}\Omega_3^2. $$

Let the intermediate control input u be given by

$$u = [u_1\ u_2\ u_3\ u_4]^{\mathrm{T}} \triangleq [\Omega_1^2\sin\mu\ \ \Omega_1^2\cos\mu\ \ \Omega_2^2\ \ \Omega_3^2]^{\mathrm{T}}. \tag{26}$$

Then, u_δ and u are related by

$$u_\delta = Mu, \tag{27}$$

where the invertible mixing matrix M is defined by

$$M \triangleq \begin{bmatrix} 0 & -K_{\mathrm{F}} & -K_{\mathrm{F}} & -K_{\mathrm{F}} \\ 0 & l_1 K_{\mathrm{F}} & -l_2 K_{\mathrm{F}} & -l_2 K_{\mathrm{F}} \\ 0 & 0 & -l_3 K_{\mathrm{F}} & l_3 K_{\mathrm{F}} \\ l_1 K_{\mathrm{F}} & -K_{\mathrm{M}} & K_{\mathrm{M}} & -K_{\mathrm{M}} \end{bmatrix}.$$

In the inner-loop controller, the control input Δu_δ, generated by RCAC, represents an increment in the control input u_δ about the initial conventional control input u_{δ_0}, that is, $\Delta u_\delta = u_\delta - u_{\delta_0}$, where $u_{\delta_0} = [\delta_{\mathrm{col}_0}\ \delta_{\mathrm{lon}_0}\ \delta_{\mathrm{lat}_0}\ \delta_{\mathrm{ped}_0}]^{\mathrm{T}}$. Note that the initial input u_{δ_0} need not be trim control. It follows from (27)

$$\Delta u = M^{-1}\Delta u_\delta, \tag{28}$$

where $\Delta u = u - u_0$, and the initial intermediate control input u_0 is given by

$$u_0 = [\Omega_{1_0}^2\sin\mu_0\ \ \Omega_{1_0}^2\cos\mu_0\ \ \Omega_{2_0}^2\ \ \Omega_{3_0}^2]^{\mathrm{T}}. \tag{29}$$

From (26), the components of the manipulated control input u_{m} are given by

$$\Omega_1^2 = \sqrt{u_1^2 + u_2^2}, \quad \Omega_2^2 = u_3, \tag{30}$$

$$\Omega_3^2 = u_4, \quad \mu = \mathrm{atan2}\Big(\frac{u_1}{u_2}\Big). \tag{31}$$

B. Outer-loop PID Controller

The three outer-loop PID controllers follow the desired horizontal position and altitude defined by a reference position vector $[X\ Y\ Z]_{\mathrm{ref}}^{\mathrm{T}}$. In particular, two PID controllers control the horizontal position $[X\ Y]_{\mathrm{ref}}^{\mathrm{T}}$ by controlling the pitch and roll angles of the tricopter, while the third PID

controller controls the altitude Z_{ref} by controlling the vertical velocity. The PID control laws for generating references for the roll angle ϕ_{ref}, pitch angle θ_{ref}, and body-z velocity w_{ref} are

$$\phi_{\mathrm{ref}} = K_{\mathrm{p}_\phi}e_{Y_{\mathrm{ref}}} + K_{\mathrm{i}_\phi}\int e_{Y_{\mathrm{ref}}}\mathrm{d}t + K_{\mathrm{d}_\phi}\frac{\mathrm{d}}{\mathrm{d}t}e_{Y_{\mathrm{ref}}}, \tag{32}$$

$$\theta_{\mathrm{ref}} = K_{\mathrm{p}_\theta}e_{X_{\mathrm{ref}}} + K_{\mathrm{i}_\theta}\int e_{X_{\mathrm{ref}}}\mathrm{d}t + K_{\mathrm{d}_\theta}\frac{\mathrm{d}}{\mathrm{d}t}e_{X_{\mathrm{ref}}}, \tag{33}$$

$$w_{\mathrm{ref}} = K_{\mathrm{pw}}e_{Z_{\mathrm{ref}}} + K_{\mathrm{iw}}\int e_{Z_{\mathrm{ref}}}\mathrm{d}t + K_{\mathrm{dw}}\frac{\mathrm{d}}{\mathrm{d}t}e_{Z_{\mathrm{ref}}}, \tag{34}$$

where $e_{Y_{\mathrm{ref}}} = Y_{\mathrm{ref}} - Y$, $e_{X_{\mathrm{ref}}} = X_{\mathrm{ref}} - X$, and $e_{Z_{\mathrm{ref}}} = Z_{\mathrm{ref}} - Z$. Note that, a negative pitch angle is required in order for the tricopter to move forward, that is, $X_{\mathrm{ref}} > 0$, hence, K_{p_θ}, K_{i_θ}, K_{d_θ} are negative. On the other hand, positive Y_{ref} and Z_{ref} require positive roll angle and z-body velocity, respectively, and thus, K_{p_ϕ}, K_{i_ϕ}, K_{d_ϕ}, K_{pw}, K_{iw} and K_{dw} are positive. The chosen PID gains are given in Table. III.

TABLE III: PID gains

	ϕ	θ	ψ
K_{p}	0.2	−0.01	0.1
K_{i}	0.2	−0.01	0.1
K_{d}	2	−0.01	0.1

C. Inner-loop RCAC

We use RCAC in the inner-loop to follow Euler angles, angular rates, and body-z velocity commands, as shown in Fig. 2. The formulation of RCAC is given in [9]. In order to construct the RCAC filter G_{f}, we linearize the nonlinear TRT dynamics $f(x, u_\delta)$ given by (3)–(7) around the hover trim condition, and define the following matrices

$$A_{\mathrm{c}} \triangleq \frac{\partial f}{\partial x}, \quad B_{\mathrm{c}} \triangleq \frac{\partial f}{\partial u_\delta}, \tag{35}$$

where the state vector is defined as

$$x \triangleq [w\ \phi\ \theta\ \psi\ p\ q\ r]^{\mathrm{T}}.$$

The matrices A_{c} and B_{c} evaluated at the trim condition are

$$A_{\mathrm{c}} = \begin{bmatrix} 0 & -g\sin\phi_{\mathrm{trim}} & 0 & 0 & 0 & 0 & 0 \\ 0 & 0 & 0 & 0 & 1 & 0 & 0 \\ 0 & 0 & 0 & 0 & 0 & \cos\phi_{\mathrm{trim}} & -\sin\phi_{\mathrm{trim}} \\ 0 & 0 & 0 & 0 & 0 & \sin\phi_{\mathrm{trim}} & \cos\phi_{\mathrm{trim}} \\ 0 & 0 & 0 & 0 & 0 & 0 & 0 \\ 0 & 0 & 0 & 0 & 0 & 0 & 0 \\ 0 & 0 & 0 & 0 & 0 & 0 & 0 \end{bmatrix}, \tag{36}$$
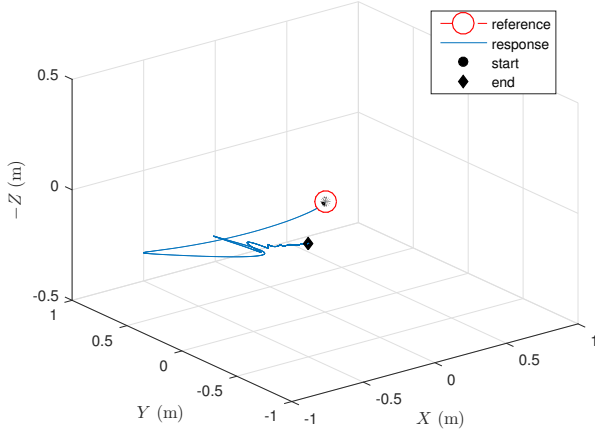
Fig. 3: Flight trajectory. The command is to hold the position at the origin. After the transient, RCAC trims the TRT in hover flight near the origin.

$$B_c = \begin{bmatrix} \frac{1}{m} & 0 & 0 & 0 \\ 0 & 0 & 0 & 0 \\ 0 & 0 & 0 & 0 \\ 0 & 0 & 0 & 0 \\ 0 & 0 & \frac{1}{I_{xx}} & 0 \\ 0 & \frac{1}{I_{yy}} & 0 & 0 \\ 0 & 0 & 0 & \frac{1}{I_{zz}} \end{bmatrix}. \tag{37}$$

We assume ϕ_{trim} is unknown to RCAC, and thus we use ϕ_0 in place of ϕ_{trim} in (36) to construct A_c. We discretize the matrices A_c and B_c using $A = e^{A_c T_s}$ and $B = A_c^{-1}(A - I)B_c$, where T_s is the sampling time.

IV. FLIGHT SIMULATION

We use the nonlinear tricopter model given in Section II to simulate the TRT dynamics. However, we use only the discretized matrices A and B given to construct G_f in RCAC. We choose $T_s = 0.01\,\text{sec}$, $k_0 = 1$, $n_c = 4$, $n_f = 1$, $R_\theta = 10^{-2}I_{l_\theta}$, $R_u = \text{diag}(10^{-2}, 10^{-2}, 10^{-4}, 10^{-4})$, and $R_z = \text{diag}(1, 10^4, 10^4, 10^4, 10, 10, 10)$.

For all examples, we initialize the TRT model with the non-trim states $[\phi\,\theta\,\psi] = [-5\,5\,0]\,\text{deg}$, $X = Y = Z = 0\,\text{m}$, $u = v = w = 0.1\,\text{m/sec}$, $p = q = r = 2\,\text{deg/sec}$ and the non-trim control inputs $\mu = 20\,\text{deg}$, $[\Omega_1\,\Omega_2\,\Omega_3] = [1400\,1300\,1300]\,\text{rpm}$. Moreover, for all of the examples, we set the reference commands $[\psi\,p\,q\,r]_{\text{ref}}$ as zero, whereas, the reference commands $[w\,\phi\,\theta]_{\text{ref}}$ are generated by the PID controllers in the outer-loop, as shown in Fig. 2.

A. Hover Flight

We set $[X\,Y\,Z]_{\text{ref}} = 0\,\text{m}$ to achieve hover flight. Fig. 3 shows that, after the transient, RCAC trims the TRT in hover flight near the origin. Fig. 4 shows the response of the TRT position. At $t = 40\,\text{sec}$, the command-following errors in X, Y, and Z are $-0.05\,\text{m}$, $0.07\,\text{m}$ and $0.19\,\text{m}$.

Figs. 5 and 6 show that, after the transient, the states and control inputs of the TRT converge close to the hover trim states and control inputs computed analytically in Section II-B and shown in Table. II. Note that the controller gains θ converge. At $t = 40\,\text{sec}$, $\phi = -11.1\,\text{deg}$, $\theta = -0.01\,\text{deg}$, $\mu = 30.49\,\text{deg}$, $\Omega_2 = \Omega_3 = 1338\,\text{rpm}$, and $\Omega_1 = 1441\,\text{rpm}$, which are close to the hover trim values given in Table II.
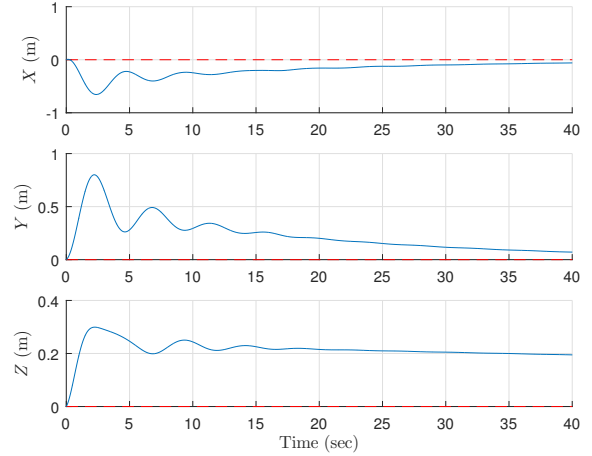
Fig. 4: Hover flight. Outer-loop PID command following. At $t = 40\,\text{sec}$, the command-following errors in X, Y, and Z are $-0.05\,\text{m}$, $0.07\,\text{m}$ and $0.19\,\text{m}$.
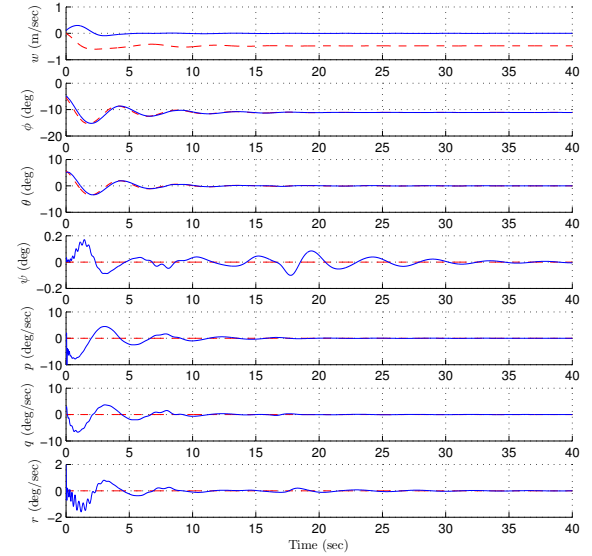
Fig. 5: Hover flight. Inner-loop RCAC command following. After the transient, the states of the TRT converge close to the hover trim states computed analytically in Section II-B and shown in Table. II.

B. Horizontal Straight Line Flight

We first trim the TRT in hover flight by commanding $[X\,Y\,Z]_{\text{ref}} = 0\,\text{m}$ up to $t = 20\,\text{sec}$, and then set $Z_{\text{ref}} = 0\,\text{m}$ and $[X\,Y]_{\text{ref}}$ to be a ramp with a slope of $2\,\text{m/sec}$ in order to fly TRT in a horizontal straight line. Fig. 7 shows that, after the transient, RCAC trims the TRT in horizontal straight line flight along the commanded trajectory. Fig. 8 shows the response of the TRT position. At $t = 60\,\text{sec}$, the command-following errors in X, Y, Z are $-0.01\,\text{m}$, $0.03\,\text{m}$ and $0.01\,\text{m}$.

Figs. 9 and 10 show that, after the transient, the states and control inputs of the TRT converge to fixed values such that the TRT achieves the commanded horizontal straight line flight. Note that the controller gains θ also converge. At $t = 60\,\text{sec}$, $\phi = -11.1\,\text{deg}$, $\theta = 0\,\text{deg}$, $\mu = 30.49\,\text{deg}$, $\Omega_2 = \Omega_3 = 1339\,\text{rpm}$, and $\Omega_1 = 1442\,\text{rpm}$.
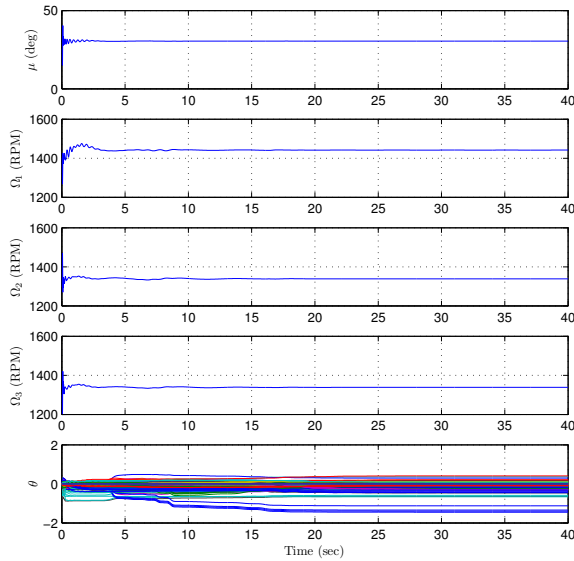
Fig. 6: Hover Flight. TRT control inputs generated by RCAC. After the transient, the control inputs converge close to the hover trim control inputs computed analytically in Section II-B and shown in Table. II. The controller gains θ also converge.
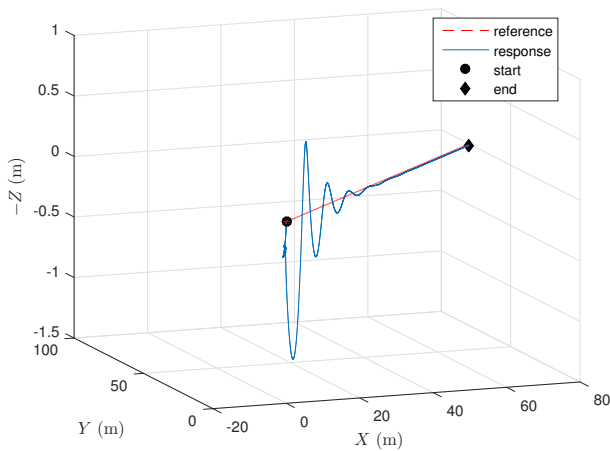
Fig. 7: Flight trajectory. The command is to fly TRT in a horizontal straight line. After the transient, RCAC trims the TRT in a horizontal straight line flight along the commanded trajectory.

C. Horizontal Circular Flight

We first trim the TRT in hover flight by commanding $[X\,Y\,Z]_{\mathrm{ref}} = 0\,\mathrm{m}$ up to $t = 20\,\mathrm{sec}$, and then set $Z_{\mathrm{ref}} = 0\,\mathrm{m}$ and $[X\,Y]_{\mathrm{ref}}$ to be a circle of radius $10\,\mathrm{m}$ with a turn-rate of $16\,\mathrm{deg/sec}$ in order to fly TRT in a horizontal circle. Fig. 11 shows that, after the transient, RCAC flies TRT along the commanded horizontal circular trajectory. Fig. 12 shows the response of the TRT position. At $t = 90\,\mathrm{sec}$, the command-following errors in X, Y, Z are $0.3\,\mathrm{m}$, $0.3\,\mathrm{m}$, $-0.1\,\mathrm{m}$.

Figs. 13 and 14 show that, after the transient, the states and control inputs of the TRT converge to harmonics such that the TRT achieves the commanded horizontal circular flight path. Note that the controller gains θ converge to fixed values.
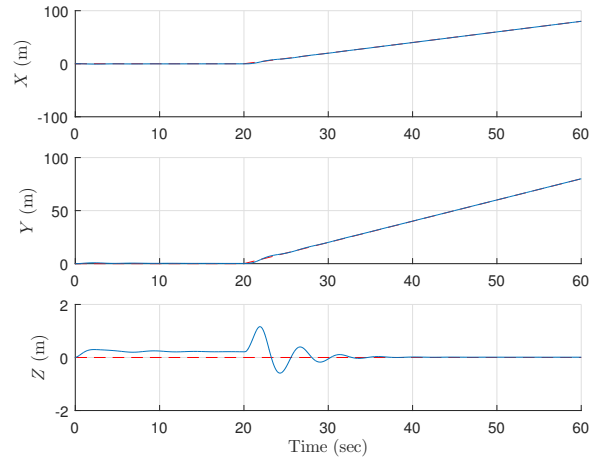
Fig. 8: Horizontal straight line flight. Outer-loop PID command following. At $t = 60\,\mathrm{sec}$, the command-following errors in X, Y, and Z are $-0.01\,\mathrm{m}$, $0.03\,\mathrm{m}$ and $0.01\,\mathrm{m}$.
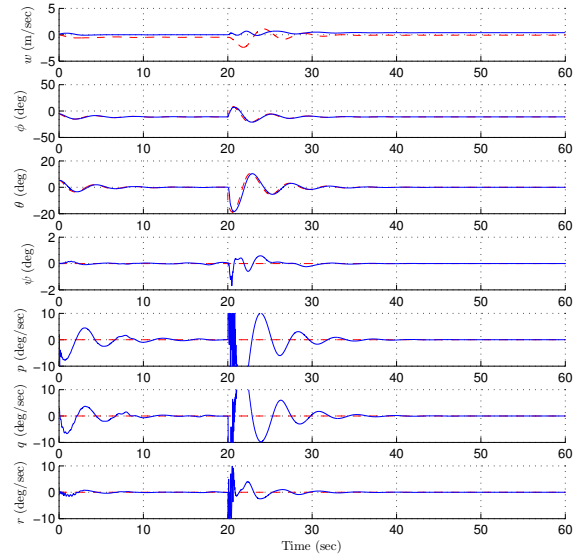
Fig. 9: Horizontal straight line flight. Inner-loop RCAC command following. After the transient, the states of the TRT converge to fixed values such that the TRT achieves the commanded horizontal straight-line flight.

V. CONCLUSIONS

This paper presented an application of retrospective cost adaptive control (RCAC) to an unconventional aircraft, namely, a tilt-rotor tricopter (TRT). An inner-outer-loop control scheme was presented, where the outer-loop consisted of PID controllers and inner-loop consisted of RCAC. We showed that RCAC was able to trim the TRT in hover flight from non-trim states and control inputs. The obtained hover trim states and control inputs using RCAC were found to be close to the analytically determined hover trim states and control inputs. We also showed the effectiveness of RCAC for flying TRT in horizontal straight-line and circular trajectories.

REFERENCES

[1] Z. T. Dydek and et al, "Adaptive Control and the NASA X-15-3 Flight Revisited: Lessons Learned and Lyapunov-stability-based Design," *IEEE Contr. Sys. Mag.*, vol. 30, pp. 32–48, 2010.

[2] N. Hovakimyan and et al, "L$_1$ Adaptive Control for Safety-Critical Systems," *IEEE Contr. Sys. Mag.*, vol. 31, pp. 54–104, 2011.
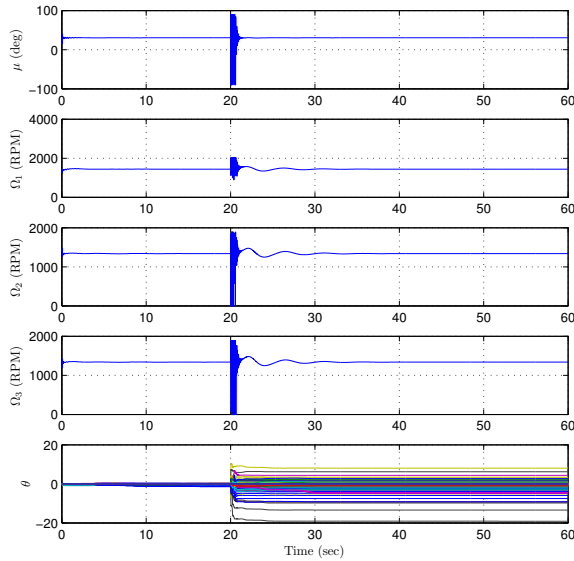
Fig. 10: Horizontal Straight-line Flight. After the transient, the control inputs of the TRT converge such that the TRT achieves horizontal straight-line flight. The RCAC controller gains θ also converge.
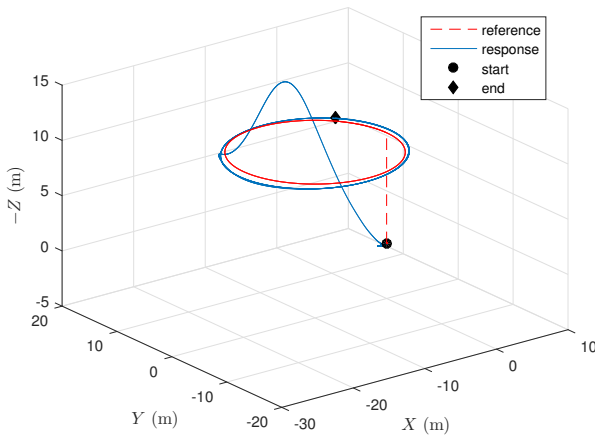
Fig. 11: Flight trajectory. The command is to fly TRT in a horizontal circle of radius $10\,\mathrm{m}$ with a turn-rate of $16\,\mathrm{deg/sec}$. After the transient, TRT flies along the commanded horizontal circular trajectory.
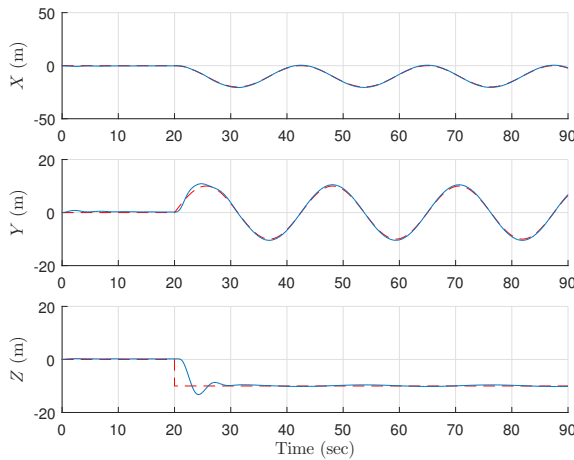
Fig. 12: Horizontal Circular Flight. Outer-loop PID command following. At $90\,\mathrm{sec}$, the errors in X, Y, Z are $0.3\,\mathrm{m}, 0.3\,\mathrm{m}, -0.1\,\mathrm{m}$.
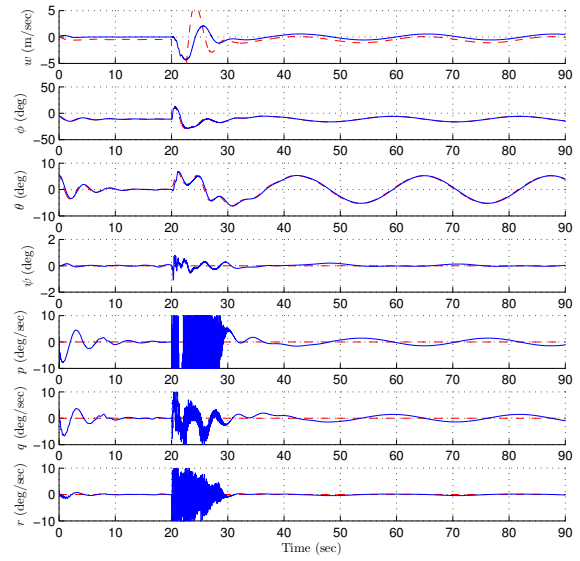
Fig. 13: Horizontal Circular Flight. Inner-loop RCAC command following. After the transient, the states of the TRT converge to harmonics such that the TRT achieves the commanded horizontal circular flight path.
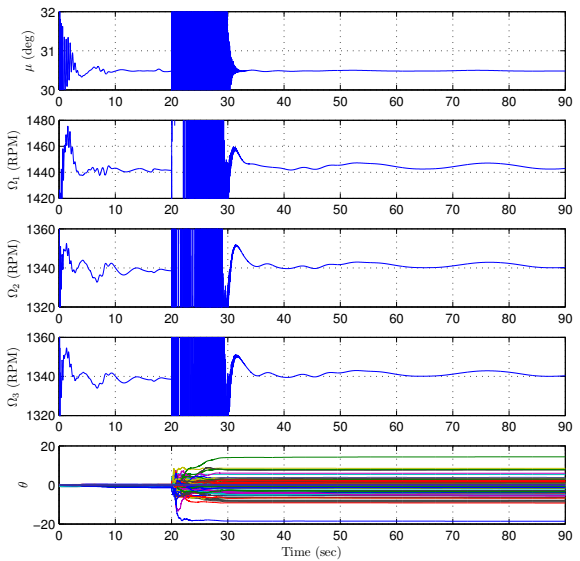
Fig. 14: Horizontal Circular Flight. TRT control inputs generated by RCAC. After the transient, the control inputs of the TRT converge to harmonics such that the TRT achieves the commanded horizontal circular flight path. The controller gains θ converge to fixed values.

[3] D.-W. Yoo and et al, "Dynamic Modeling and Control System Design for Tri-Rotor UAV," in *Proc. ISCAA*, Harbin, China, 2010, pp. 762–767.

[4] M. A. Santillo and D. S. Bernstein, "Adaptive Control Based on Retrospective Cost Optimization," *J. Guid. Contr. Dyn.*, vol. 33, pp. 289–304, 2010.

[5] J. B. Hoagg and D. S. Bernstein, "Retrospective Cost Model Reference Adaptive Control for Nonminimum-Phase Systems," *J. Guid. Contr. Dyn.*, vol. 35, pp. 1767–1786, 2012.

[6] Y. Rahman, A. Xie, J. B. Hoagg, and D. S. Bernstein, "A Tutorial and Overview of Retrospective-Cost-Based Adaptive Control," in *Proc. Amer. Contr. Conf.*, Boston, MA, July 2016, pp. 3386–3409.

[7] F. M. Sobolic and D. S. Bernstein, "Aerodynamic-Free Adaptive Control of the NASA Generic Transport Model," *AIAA GNC*, 2013.

[8] A. Ansari, M.-J. Yu, and D. S. Bernstein, "Exploration and Mapping of an Unknown Flight Envelope," in *IEEE CDC*, 2014, pp. 523–528.

[9] A. Ansari and D. S. Bernstein, "Retrospective Cost Adaptive Control of Generic Transport Model Under Uncertainty and Failure," *J. Aero. Info. Sys.*, 2017 (in press).

[10] R. F. Stengel, *Flight Dynamics*. Princeton University Press, 2004.